A system-level calibration method including temperature-related error coefficients for a strapdown inertial navigation system

OPEN ACCESS
IOP Publishing
Measurement Science and Technology
Meas. Sci. Technol. **32** (2021) 115117 (9pp)
https://doi.org/10.1088/1361-6501/ac0acd

A system-level calibration method including temperature-related error coefficients for a strapdown inertial navigation system

Zichao Wang, Yuanping Xie*, Xudong Yu, Huiying Fan, Guo Wei, Lin Wang, Zhenfang Fan, Guochen Wang and Hui Luo

College of Advanced Interdisciplinary Studies, National University of Defense Technology, Changsha 410073, People's Republic of China

E-mail: xyp99999@139.com

Received 18 March 2021, revised 10 May 2021
Accepted for publication 11 June 2021
Published 29 July 2021

Abstract

The calibration of error coefficients for accelerometers and laser gyros is an effective way to improve the navigation precision of strapdown inertial navigation systems. The calibration parameters often change with temperature. This paper proposes a system-level calibration method including temperature-related error coefficients. The method includes an improved 18-step calibration scheme with temperature being changed by using a thermal chamber. A 42-dimensional Kalman filter is applied to estimate the error parameters including the bias, scale factor errors, installation errors and temperature-related error coefficients of accelerometers. This method has the great advantage of simplifying the calibration procedure and is widely applicable to all temperature-related error coefficients. Compared with the traditional calibration method at different temperature points, the calibration time of the proposed method is shortened by 24 h. The feasibility of this method is verified by simulations and navigation experiments. The results of navigation experiments show that the maximum positioning errors in pure inertial navigation decrease by approximately 30% after temperature compensation.

Keywords: strapdown inertial navigation system, system-level calibration, Kalman filter temperature compensation

(Some figures may appear in colour only in the online journal)

1. Introduction

Strapdown inertial navigation systems (SINSs) are widely used in the field of navigation. An inertial measurement unit (IMU) is the core component of a SINS. A laser gyro and quartz flexible accelerometer are the most common inertial sensors in IMUs [1]. Due to the error of scale factors of inertial sensors and installation errors casued by the IMU assembly process, the real relationship between the IMU's input and output does not satisfy the idealized physical equations. Thus it is necessary to calibrate the value of error parameters in order to establish an accurate mathematical relationship between the IMU's input and output.

The traditional calibration method includes separated calibration and system-level calibration. The separated calibration method uses a high-precision turntable to give an accurate reference for the basis of orientation, position and angular velocity. By maintaining the IMU in different positions with respect to the local gravitational acceleration and the angular

* Author to whom any correspondence should be addressed.

rate of the Earth, it is possible to calibrate the error terms of the gyroscope and accelerometers [2, 3]. However, the performance of this method in terms of accuracy is fundamentally limited by the precision of the turntable [4]. Use of a more sophisticated turntable will increase the cost of calibration.

In order to overcome the disadvantages of separated calibration, a system-level calibration method has been proposed. This method makes estimates of the error parameters based on the error of navigation measurements. Also, this method is not limited by the accuracy of the turntable and can make full use of the rotating mechanism of the rotating inertial navigation system to achieve self-calibration. Many researchers have carried out studies on system-level calibration. Camberlein *et al* [5] put forward a calibration path with 19 positions which could achieve the required accuracy within 20 min. Wang *et al* [6] designed a 24-dimensional error state Kalman filter to improve the accuracy of system-level calibration. Pan *et al* [7] proposed an accurate calibration method for the nonlinear scale factor of the accelerometer by estimating the rates of change of velocity errors. Yuan *et al* [8] designed a 16-position rotation scheme for a dual-axis rotational INS.

In most instances, the calibration parameters are considered to have a constant value. However, as the output of a quartz flexible accelerometer is sensitive to the working temperature [9–12], the calibration parameters of the accelerometer are required to be compensated to eliminate the error caused by temperature change. The traditional temperature compensation method has two main aspects: device-level solutions and temperature model identification [11]. Yang *et al* [13] used a temperature stabilization chamber to control the working temperature of a SINS. Some researchers have tried to find temperature-insensitive materials for inertial sensors [14].

These device-level methods are costly and require extensive research [15]. Therefore, this paper mainly focuses on temperature model identification.

Polynomial regression methods have been widely used to establish a temperature model for the calibration parameters of IMUs [12]. In [16–18] a temperature model was built by calculating the coefficients of each temperature point by least-squares fitting. Liao and Li [19] used third-order polynomials to compensate the bias error of an accelerometer. In [20, 21] a discrete calibration method was used to identify a temperature model; this required the temperature to be kept stable for more than 3 h at each temperature point. All these methods require multi-group calibration experiments at different temperature points. The calibration procedure is therefore complicated and time-consuming.

In order to overcome these shortcomings of traditional calibration methods, this paper proposes a system-level calibration method including temperature-related error coefficients. This method introduces the temperature-related error coefficients of the accelerometer into the traditional IMU error model. Furthermore, an improved 18-step calibration scheme which uses a thermal chamber to change temperature. This method needs only one calibration experiment to estimate the bias, scale factor errors, installation errors and temperature error coefficients of accelerometers within 4.2 h. Compared with temperature compensation based on least-squares fitting, the proposed method has a simple and time-saving calibration procedure. Moreover, the proposed method is feasible for temperature compensation of all error parameters of an accelerometer.

The rest of this paper is organized as follows. Section 2 defines the coordinate systems, error parameters and error model for an IMU. Section 3 constructs a 42-dimensional Kalman filter and introduces the improved 18-step calibration scheme. Section 4 shows the simulation results and analyses the feasibility of the proposed method. Experimental results and analysis are given in section 5. Finally, section 6 gives our conclusion.

2. An IMU error model including temperature-related error coefficients

The coordinate frames used in this paper contain the inertial frame (i-frame), the earth frame (e-frame), the navigation frame (n-frame, defined as north–east–down) and the body frame (b-frame, defined as right–forward–upward).

For medium- and high-precision quartz flexible accelerometers it is necessary to consider the thermal drift errors of scale factor, installation relationship and constant bias caused by temperature change. Considering that the thermal drift errors of laser gyros are compensated before the assembly of the IMU and have less impact on the calibration results, this paper proposes an IMU error model which contains only temperature error coefficients of the accelerometer and takes no account of the gyro's temperature model.

The error model of the accelerometer is presented as

$$\begin{aligned}
&\begin{bmatrix} \delta f_x^b \\ \delta f_y^b \\ \delta f_z^b \end{bmatrix} \\
&= \begin{bmatrix} B_{ax} \\ B_{ay} \\ B_{az} \end{bmatrix} + \begin{bmatrix} \Delta T_{ax} * TB_{ax} \\ \Delta T_{ay} * TB_{ay} \\ \Delta T_{az} * TB_{az} \end{bmatrix} \\
&+ \begin{bmatrix} \delta K_{ax} & \delta M_{axy} & \delta M_{axz} \\ \delta M_{ayx} & \delta K_{ay} & \delta M_{ayz} \\ \delta M_{azx} & \delta M_{azy} & \delta K_{az} \end{bmatrix} \begin{bmatrix} f_x^b \\ f_y^b \\ f_z^b \end{bmatrix} \\
&+ \begin{bmatrix} \Delta T_{ax} * TK_{ax} & \Delta T_{ay} * TM_{axy} & \Delta T_{az} * TM_{axz} \\ \Delta T_{ax} * TM_{ayx} & \Delta T_{ay} * TK_{ay} & \Delta T_{az} * TM_{ayz} \\ \Delta T_{ax} * TM_{azx} & \Delta T_{ay} * TM_{azy} & \Delta T_{az} * TK_{az} \end{bmatrix} \begin{bmatrix} f_x^b \\ f_y^b \\ f_z^b \end{bmatrix}
\end{aligned} \tag{1}$$

where f_i^b is the actual value of the specific force in the b-frame which contains no errors along axis i, δf^b is the error of the specific force, B_{ai} is the constant bias of the accelerometer along axis i, $TB_{ai}$is the first-order temperature coefficient of the accelerometer bias, δK_{ai} is the scale factor error of the accelerometer along axis i and $TK_{ai}$is the first-order temperature coefficient of the scale factor error of the accelerometer. $\delta M_{aij}(i = x, y, z, j = x, y, z, i \neq j)$ is the accelerometer installation error between axis i and plane oij of the b-frame, TM_{aij} is the first-order temperature coefficient of the installation errors and ΔT_{ai} is the working temperature rate at the surface of the accelerometer along axis i.

The error model of the laser gyro is presented as

$$\begin{bmatrix} \delta\omega^b_{ibx} \\ \delta\omega^b_{iby} \\ \delta\omega^b_{ibz} \end{bmatrix} = \begin{bmatrix} B_{gx} \\ B_{gy} \\ B_{gz} \end{bmatrix} + \begin{bmatrix} \delta K_{gx} & 0 & 0 \\ \delta M_{gyx} & \delta K_{gy} & 0 \\ \delta M_{gzx} & \delta M_{gzy} & \delta K_{gz} \end{bmatrix} \begin{bmatrix} \omega^b_{ibx} \\ \omega^b_{iby} \\ \omega^b_{ibz} \end{bmatrix} \quad (2)$$

where ω^b_{ibj} is the actual value of the angular rate in the b-frame which contains no errors along axis j, $\delta\omega^b_{ib}$ is the error of the angular rate, B_{gi} is the constant drift of the gyro along axis i and δK_{gi} is the scale factor error of the gyro along axis i. $\delta M_{gij}(i = y,z,j = x,y,i \neq j)$ is the gyro's installation error between axis i and plane oij of the b-frame.

Based on the error model of the accelerometer in equation (1), the error compensation model of the accelerometer bias, scale factor and installation matrix including temperature error coefficients is presented as

$$\begin{aligned} \begin{bmatrix} K_{ax} & 0 & 0 \\ 0 & K_{ay} & 0 \\ 0 & 0 & K_{az} \end{bmatrix} &= \begin{bmatrix} \tilde{K}_{ax} & 0 & 0 \\ 0 & \tilde{K}_{ay} & 0 \\ 0 & 0 & \tilde{K}_{az} \end{bmatrix} \\ &- \begin{bmatrix} \delta K_{ax} & 0 & 0 \\ 0 & \delta K_{ay} & 0 \\ 0 & 0 & \delta K_{az} \end{bmatrix} \begin{bmatrix} \tilde{K}_{ax} & 0 & 0 \\ 0 & \tilde{K}_{ay} & 0 \\ 0 & 0 & \tilde{K}_{az} \end{bmatrix} \\ &- \begin{bmatrix} \Delta T_{ax} * TK_{ax} & 0 & 0 \\ 0 & \Delta T_{ay} * TK_{ay} & 0 \\ 0 & 0 & \Delta T_{az} * TK_{az} \end{bmatrix} \\ &\times \begin{bmatrix} \tilde{K}_{ax} & 0 & 0 \\ 0 & \tilde{K}_{ay} & 0 \\ 0 & 0 & \tilde{K}_{az} \end{bmatrix} \end{aligned} \quad (3)$$

where K_a is the scale factor of the accelerometer after compensation and $\tilde{K}_a$ is the scale factor of the accelerometer with errors

$$\begin{aligned} \begin{bmatrix} 0 & M_{axy} & M_{axz} \\ M_{ayx} & 0 & M_{ayz} \\ M_{azx} & M_{azy} & 0 \end{bmatrix} &= \begin{bmatrix} 0 & \tilde{M}_{axy} & \tilde{M}_{axz} \\ \tilde{M}_{ayx} & 0 & \tilde{M}_{ayz} \\ \tilde{M}_{azx} & \tilde{M}_{azy} & 0 \end{bmatrix} \\ &- \begin{bmatrix} 0 & \delta M_{axy} & \delta M_{axz} \\ \delta M_{ayx} & 0 & \delta M_{ayz} \\ \delta M_{azx} & \delta M_{azy} & 0 \end{bmatrix} \begin{bmatrix} \tilde{K}_{ax} & 0 & 0 \\ 0 & \tilde{K}_{ay} & 0 \\ 0 & 0 & \tilde{K}_{az} \end{bmatrix} \\ &- \begin{bmatrix} 0 & \Delta T_{ay} * TM_{axy} & \Delta T_{az} * TM_{axz} \\ \Delta T_{ax} * TM_{ayx} & 0 & \Delta T_{az} * TM_{ayz} \\ \Delta T_{ax} * TM_{azx} & \Delta T_{ay} * TM_{azy} & 0 \end{bmatrix} \\ &\times \begin{bmatrix} \tilde{K}_{ax} & 0 & 0 \\ 0 & \tilde{K}_{ay} & 0 \\ 0 & 0 & \tilde{K}_{az} \end{bmatrix} \end{aligned} \quad (4)$$

M_a is the installation matrix of the accelerometer after compensation $\tilde{M}_a$ is the installation matrix of the accelerometer with errors.

$$\begin{bmatrix} B_{ax} \\ B_{ay} \\ B_{az} \end{bmatrix} = \begin{bmatrix} \tilde{B}_{ax} \\ \tilde{B}_{ay} \\ \tilde{B}_{az} \end{bmatrix} + \begin{bmatrix} \Delta T_{ax} * TB_{ax} \\ \Delta T_{ay} * TB_{ay} \\ \Delta T_{az} * TB_{az} \end{bmatrix} \quad (5)$$

where B_a is the constant bias of the accelerometer after compensation $\tilde{B}_a$ is the constant bias of the accelerometer with errors.

3. The system-level calibration with a 42-dimensional Kalman filter

3.1. Construction of the Kalman filter

In order to calibrate the error parameters of the IMU error model, this paper applies the system-level calibration method using a 42-dimensional Kalman filter. The main function of the Kalman filter is to estimate the parameters of the IMU error model by observing the velocity and position errors of navigation. Based on the form of the traditional navigation error equation, this paper expands the velocity error equation which contains the temperature error coefficients of the accelerometer:

$$\begin{aligned} &\dot{\phi} = \phi \times \omega^n_{in} + \delta\omega^n_{in} - C^n_b([\delta K_g] + [\delta M_g])\omega^b_{ib} - B^n_g \\ &\delta\dot{V}^n = -\phi^n \times f^n + C^n_b([\delta K_a] + T * [TK_a] + [\delta M_a] + T * [TM_a])f^b \\ &+ \delta V^n \times (2\omega^n_{ie} + \omega^n_{en}) + V^n \times (2\delta\omega^n_{ie} + \delta\omega^n_{en}) + B^n_a + T * TB^n_a \\ &\delta\dot{L} = \frac{\delta V_N}{R_N + h} - \delta h \frac{V_N}{(R_N + h)^2} \\ &\delta\dot{\lambda} = \frac{\delta V_E}{R_E + h}\sec L + \delta L \frac{V_E}{R_E + h}\tan L \sec L - \delta h \frac{V_E \sec L}{(R_E + h)^2} \\ &\delta h = -\delta V_D \end{aligned} \quad (6)$$

where $V^n = \begin{bmatrix} V^n_N & V^n_E & V^n_D \end{bmatrix}^T$ denotes the velocity of the IMU in the n-frame and L, λ and h denote the latitude, longitude and altitude, respectively. $\phi^n = \begin{bmatrix} \phi^n_N & \phi^n_E & \phi^n_D \end{bmatrix}^T$ denotes the attitude error in the n-frame, $\omega^n_{ie} = \begin{bmatrix} \omega_{ie}\cos L & 0 & -\omega_{ie}\sin L \end{bmatrix}^T$ denotes the angular rate of the earth in the n-frame and $\omega^n_{en} = \begin{bmatrix} \frac{V_E}{R_E+h} & -\frac{V_N}{R_N+h} & \frac{V_E \tan L}{R_E+h} \end{bmatrix}$ denotes the angular rate of the n-frame related to the e-frame. R_N, R_E denote the meridian radius of the earth and δ [•] denotes the error of the vector [•].

We expand equation (6) and rewrite it in the form of a state equation. The state equation of the Kalman filter is presented as

$$\dot{X} = FX + W(t). \quad (7)$$

In equation (7), the state vector X consists of 42 state variables

$$\begin{aligned} X = \begin{bmatrix} \varphi_N & \varphi_E & \varphi_D & \delta V_N & \delta V_E & \delta V_D & \delta L & \delta\lambda & \delta h \\ B_{gx} & B_{gy} & B_{gz} & B_{ax} & B_{ay} & B_{az} & \delta K_{gx} & \delta M_{gyx} & \delta M_{gzx} \\ \delta K_{gy} & \delta M_{gzy} & \delta K_{gz} & \delta K_{ax} & \delta M_{ayx} & \delta M_{azx} & \delta M_{axy} & \delta K_{ay} \\ \delta M_{azy} & \delta M_{axz} & \delta M_{ayz} & \delta K_{az} & TB_{ax} & TB_{ay} & TB_{az} & TK_{ax} \\ TK_{ay} & TK_{az} & TM_{ayx} & TM_{azx} & TM_{axy} & TM_{azy} & TM_{axz} \\ TM_{ayz} \end{bmatrix}^T. \end{aligned} \quad (8)$$

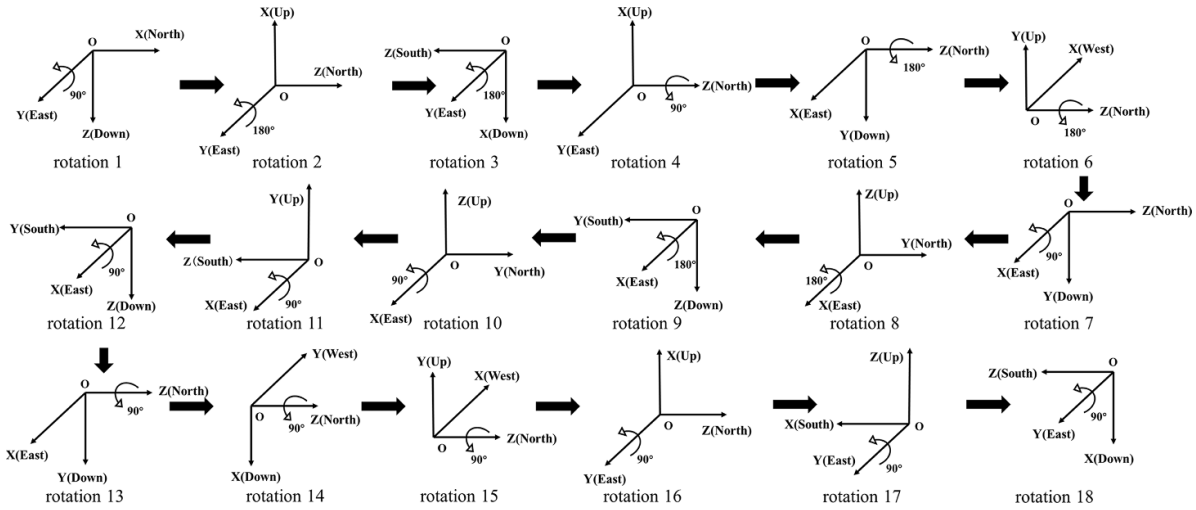

Figure 1. The 18-step rotation scheme.

The state transition matrix F is defined by equation (6). $W(t)$ is the output noise of the laser gyro and accelerometer. It is regarded as white noise.

The measurement equation of the Kalman filter is

$$Z = HX + v(t). \tag{9}$$

$v(t)$ is the measurement noise, which is regarded as white noise.

In this paper, velocity errors and position errors are selected as measurements. So the variables of the measurement vector Z and measurement matrix H are presented as

$$Z = \begin{bmatrix} \delta V_N & \delta V_E & \delta V_D & \delta L & \delta\lambda & \delta h \end{bmatrix}^T \tag{10}$$

$$H = \begin{bmatrix} 0_{3\times3} & I_{3\times3} & 0_{3\times3} & 0_{3\times33} \\ 0_{3\times3} & 0_{3\times3} & I_{3\times3} & 0_{3\times33} \end{bmatrix}_{6\times42} \tag{11}$$

where $I_{3\times3}$ denotes the identity matrix.

3.2. System-level calibration rotation scheme

This paper proposes an improved 18-step rotation scheme. This rotation scheme has been proved to be effective in calibrating the constant bias, scale factor errors and installation errors of IMUs [5]. In order to calibrate the temperature error coefficients of accelerometers, we mounted the IMU on a three-axis turntable with a thermal chamber and heated the IMU up at a constant rate during the entire calibration process. A schematic diagram of the 18-step rotation scheme is illustrated in figure 1. The rotation rate was $9^\circ\ s^{-1}$.

4. Simulation results and analysis

Simulation was carried out to verify the improved calibration scheme with temperature change. The initial velocity and attitude angle were both zero. The initial location was 112.99°E, 28.22°N and the initial alignment time was 20 min. In order to fully excite error parameters, the 18-step calibration scheme was conducted four times. The total simulation time was 4.2 h and the updating period for the sensor data and filter period were both set as 5 ms. The simulated temperature of the accelerometers increased from 0 °C at a rate of 10 °C h^{-1}.

Kalman filtering estimation curves are plotted in figure 2. All the error parameters converge to some certain values at the end of the calibration process. Table 1 shows the preset values and estimation values of error coefficients in the simulation. According to the simulation results, the proposed calibration method has a high estimation precision with a residual error close to zero. The feasibility of the proposed method was verified. We then conducted calibration experiments and navigation experiments to test the effectiveness of this method.

5. Experimental results and analysis

5.1. Calibration experiments

As shown in figure 3, the calibration experiment was carried out on a three-axis turntable with a thermal chamber. The angular resolution of turntable was better than 1 arcsec. A high-precision IMU with three laser gyros and three quartz flexible accelerometers was mounted in the thermal chamber for calibration. The bias stability of the gyros and accelerometers was $0.005^\circ\ h^{-1}$ and 20 μg respectively. A platinum resistance thermometer was mounted on each accelerometer to measure the temperature.

The experiment was conducted according to the flow diagram in figure 4. Figure 5 shows the output of the IMU and the temperature curves of the accelerometers in one calibration experiment. Considering that the temperature error coefficients need a relatively long period to converge to certain values, the 18-step calibration scheme was conducted four times in one experiment. The temperature of thermal chamber rose from 0 °C at the rate of 10 °C h^{-1}. Due to the uneven heat distribution and the delayed effect of heat transfer, the

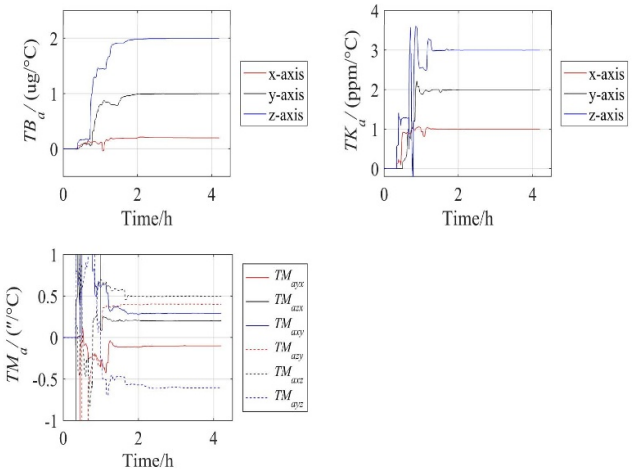

(a) Kalman filtering estimation curves of temperature error coefficients

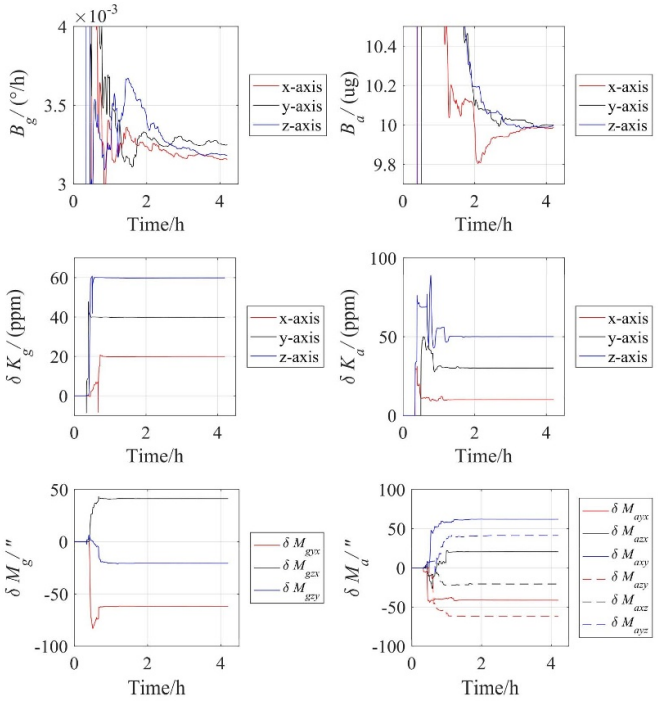

(b)Kalman filtering estimation curves of bias, scale factor error and installation error

Figure 2. Kalman filtering estimation curves in simulation.

Table 1. The preset values and estimation values of error coefficients in simulation.

Error coefficients	Preset value	Estimation value	Residual error	Error coefficients	Preset value	Estimation value	Residual error
B_{gx}(° h^{-1})	0.003	0.003 16	0.000 16	TB_{ax}(μg °C^{-1})	0.2	0.1982	0.0018
B_{gy}(° h^{-1})	0.003	0.003 26	0.000 26	TB_{ay}(μg °C^{-1})	1	0.9932	0.0068
B_{gz}/(° h^{-1})	0.003	0.003 02	0.000 02	TB_{az}(μg °C^{-1})	2	1.999	0.0010
δK_{gx}ppm)	20	20.03	0.03	TK_{ax}(ppm °C^{-1})	1	1.001	0.001
δK_{gy}ppm)	40	39.93	0.07	TK_{ay}(ppm °C^{-1})	2	1.999	0.001
δK_{gz} (ppm)	60	60.02	0.02	TK_{az}(ppm °C^{-1})	3	2.999	0.001
δM_{gyx} ('')	−61.88	−61.78	0.10	TM_{ayx}('' °C^{-1})	−0.1	−0.098	0.002
δM_{gzx} ('')	41.25	41.26	0.01	TM_{azx}('' °C^{-1})	0.2	0.202	0.002
δM_{gzy} ('')	−20.63	−20.64	0.01	TM_{axy}('' °C^{-1})	0.3	0.297	0.003
B_{ax} (μg)	1	0.99	0.01	TM_{azy}('' °C^{-1})	0.4	0.399	0.001
B_{ay} (μg)	1	1.02	0.02	TM_{axz}('' °C^{-1})	0.5	0.500	0
B_{az} (μg)	1	1.01	0.01	TM_{ayz}('' °C^{-1})	−0.6	−0.601	0.001
δK_{ax} (ppm)	10	10.07	0.06	δM_{azy} ('')	−61.88	−61.89	0.01
δK_{ay}/ppm	30	30.08	0.08	δM_{axz} ('')	−20.62	−20.59	0.03
δK_{az} (ppm)	50	50.02	0.02	δM_{ayz} ('')	41.25	41.26	0.01
δM_{ayx} ('')	−41.25	−41.22	0.03	—	—	—	—
δM_{azx} ('')	20.62	20.64	0.02	—	—	—	—
δM_{axy} ('')	61.88	61.95	0.07	—	—	—	—

temperatures of the three accelerometers were different from the thermal chamber and were indicated by platinum resistance thermometers.

The Kalman filtering estimation curves of three calibration experiments are shown in figure 6. All temperature error parameters converge to some certain values and the estimated values show great consistency over three repeated experiments. Table 2 shows the standard deviation (STD) of error parameters in the three experiments. The STDs of installation errors and scale factor errors are less than 1 arcsec and 5 ppm, respectively. The STDs of the temperature error coefficients are less than 0.2 μg, 1 ppm and 0.01 arcsec, respectively. Thus, the error parameters have been identified with high repeatability.

Furthermore, a temperature model based on least-squares fitting method was researched for comparison. We set four

Figure 3. The three-axis turntable with thermal chamber and the IMU for the calibration experiment.

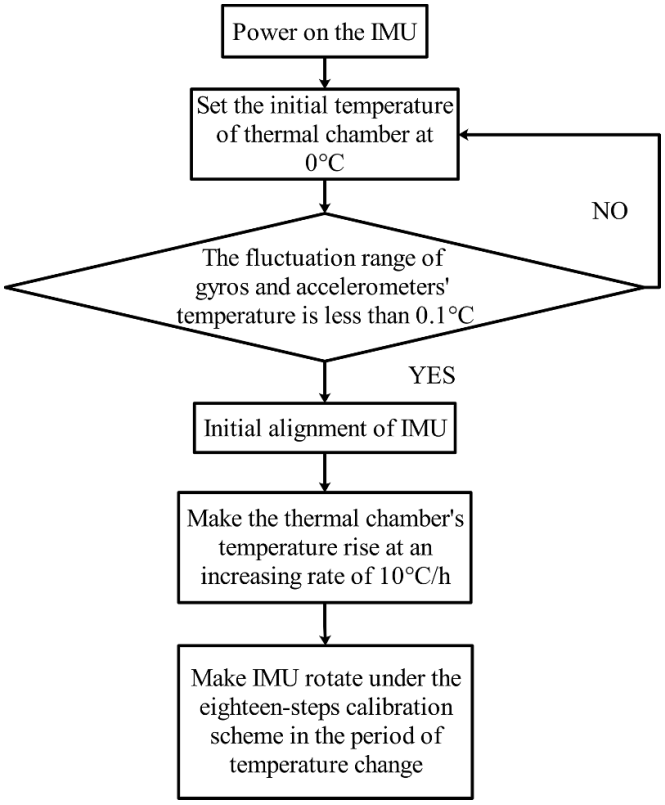

Figure 4. Flow diagram of the calibration experiment.

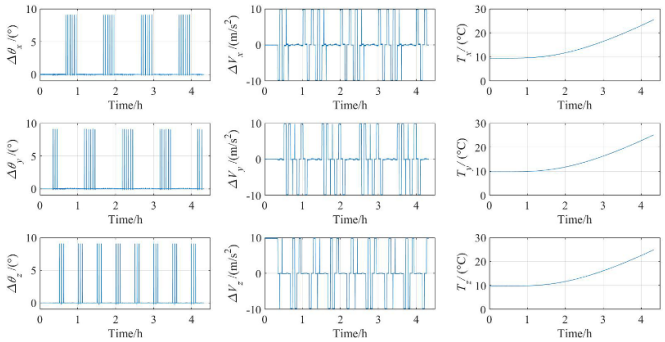

Figure 5. Output of the IMU and temperature curves of the accelerometers in one calibration experiment.

temperature points for the thermal chamber at 10 °C, 20 °C, 30 °C and 40 °C and assumed that the biases, scale factor errors and installation errors of accelerometer would be treated with the same temperature model as in equation (1). The system-level calibration based on the 18-step rotation scheme was performed at each temperature point. According to the first-order linear relationship between error coefficients and temperature points, the temperature error coefficients are solved. The calibration scheme at each temperature point requires 4.2 h. The working temperature of accelerometers needs more than 3 h to change from one temperature point to another and stay stable. The total calibration time was more than 28.8 h. Table 3 shows the temperature error coefficients based on the proposed method and the least-squares fitting method, respectively.

5.2. Navigation experiments

In order to verify the effect of the proposed system-level temperature calibration method, we used a 30-dimensional Kalman filter to calibrate the error parameters without temperature compensation under the same 18-step calibration scheme. We carried out the navigation experiments with temperature change in stationary and vibration environments based on the same three-axis turntable as in figure 3. The thermal chamber was used to control the sustained temperature drop and fluctuations in the navigation experiment. The vibration patterns are shown in table 4. First, the IMU remained stationary for 5 h. Then, the IMU vibrated in three patterns, respectively, with a 1 h stationary state between three patterns. The whole navigation time was approximately 15 h. In order to verify the proposed calibration method, the navigation experiment was carried out three times. The angular increment and specific force increment of the experiment are shown in figure 7. Figure 8 shows the temperature change of the accelerometers in three navigation experiments.

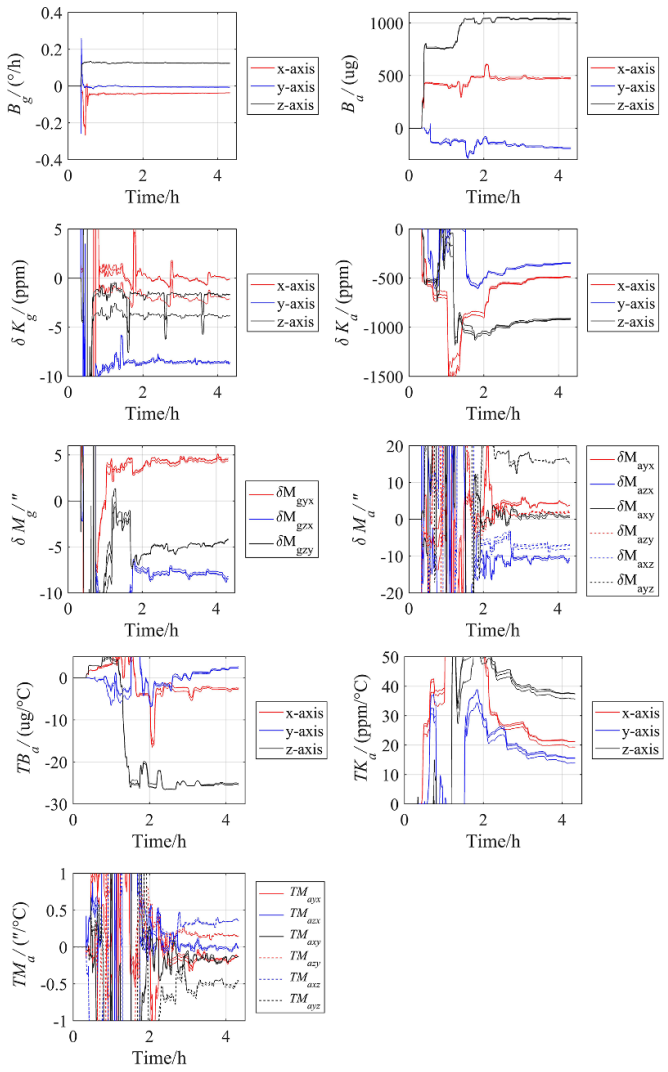

Figure 6. The Kalman filtering estimation curves in the calibration experiments.

Table 2. Standard deviation (STD) of error parameters in three experiments.

Parameters	STD
Gyro drifts (° h^{-1})	0.00028/0.00057/0.00024
Gyro scale factor errors (ppm)	0.94/0.05/1.03
Gyro installation errors (″)	0.11/0.12/0.03
Accelerometer biases (μg)	4.33/4.12/4.07
Accelerometer scale factor errors (ppm)	2.26/3.60/4.59
Accelerometer installation errors (″)	0.03/0.26/0.18/0.20/0.54/0.13
Temperature coefficients of biases (μg $°C^{-1}$)	0.15/0.13/0.12
Temperature coefficients of scale factor errors (ppm $°C^{-1}$)	0.89/0.78/0.86
Temperature coefficients of installation errors (″ $°C^{-1}$)	0.0036/0.0063/0.0016/0.0030/0.0039/0.0073

A comparison of the horizontal positioning error between the calibration parameters with and without temperature compensation is shown in figure 9. The maximum positioning error with temperature compensation in 15 h is less than 2.2 nautical miles while the positioning error without temperature compensation is more than 3.3 nautical miles. Meanwhile, the improvement in positioning precision of the two temperature compensation methods is almost the same. The calibration of temperature error coefficients based on the least-squares fitting method takes 28.8 h, while the proposed system-level calibration method takes only 4.2 h. The proposed calibration method is further proved to be effective in temperature compensation

Table 3. Temperature error coefficients for the two methods.

	Proposed method	Least-squares fitting method
Temperature coefficients of biases (μg °C)	−2.77/2.63/−25.45	−1.33/2.78/−29.38
Temperature coefficients of scale factor errors (ppm $°C^{-1}$)	19.33/13.96/35.58	17.39/13.15/32.65
Temperature coefficients of installation errors (″ $°C^{-1}$)	−0.12/−0.02/−0.13/0.14/0.37/−0.47	−0.22/−0.01/−0.08/0.23/0.32/−0.55

Table 4. Vibration patterns.

	Vibration axis (IMU)	Amplitude (°)	Period (s)	
Vibration pattern 1	*x*-axis	2	0.1	The IMU vibrates along three axes together in each pattern
	y-axis	4	0.2	
	z-axis	2	0.3	
Vibration pattern 2	*x*-axis	6	0.1	
	y-axis	5	0.2	
	z-axis	6	0.15	
Vibration pattern 3	*x*-axis	8	0.2	
	y-axis	9	0.1	
	z-axis	15	0.15	

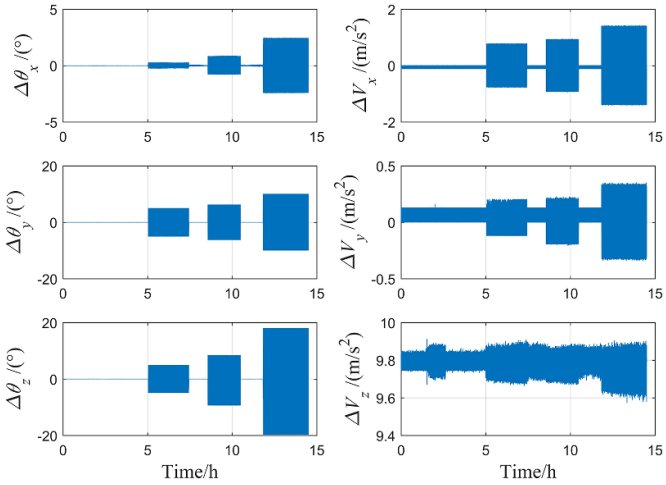

Figure 7. The angular increment and specific force increment of the navigation experiment.

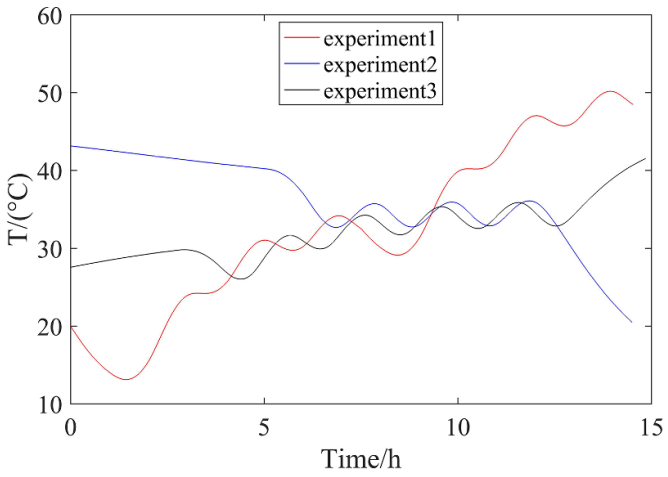

Figure 8. The temperature curve of accelerometers in the navigation experiments.

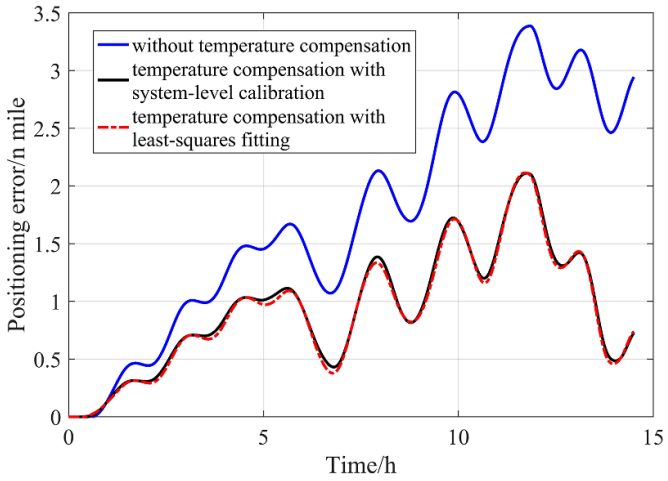

Figure 9. The comparison on horizontal positioning error between the calibration parameters with and without temperature compensation.

Table 5. The summary of experimental results.

Experiment group	Maximum positioning errors (nautical miles)		Navigation precision improvement
	With temperature compensation	Without temperature compensation	
1	2.11	3.38	37.57%
2	2.65	3.70	28.38%
3	2.27	3.74	39.30%

and time-saving. The results of three groups of experiments are shown in table 5.

6. Conclusion

A system-level calibration method including temperature error coefficients for SINS is proposed in this paper. An IMU error model including temperature error coefficients and the temperature compensation method for the calibration parameters is illustrated with specific equations. In this method, an 18-step rotation scheme has been improved with changing temperature by using a thermal chamber. The 42-dimensional Kalman filter can estimate all the calibration parameters including temperature error coefficients in one calibration experiment under the improved 18-step calibration scheme; thus the calibration process is greatly simplified and quicker. Compared with the calibration of temperature error coefficients based on least-squares fitting, the calibration time is shortened by 24 h. The simulation and the navigation experiments both prove that the proposed calibration method is effective in temperature compensation. The maximum positioning errors in pure inertial navigation decreases by 30% after temperature compensation.

Data availability statement

The data that support the findings of this study are available upon reasonable request from the authors.

ORCID iDs

Zichao Wang https://orcid.org/0000-0001-8346-7033
Xudong Yu https://orcid.org/0000-0002-3082-0830

References

[1] Farooq M and Bruder S 1989 Autonomous fault-tolerant attitude reference system using DTGs in symmetrically skewed configuration *IEEE Trans. Aerosp. Electron. Syst.* **25** 302–7
[2] Ren Q, Wang B, Deng Z H and Fu M Y 2014 A multi-position self-calibration method for dual-axis rotational inertial navigation system *Sens. Actuators* A **219** 24–31
[3] Nieminen T, Kangas J, Suuriniemi S and Kettunen L 2010 An enhanced multi-position calibration method for consumer-grade inertial measurement units applied and tested *Meas. Sci. Technol.* **21** 105204
[4] Zhang H L, Wu Y X, Wu W Q, Wu M P and Hu X P 2010 Improved multi-position calibration for inertial measurement units *Meas. Sci. Technol.* **21** 015107
[5] Camberlein L and Mazzanti F 1985 Calibration technique for laser gyro strapdown inertial navigation systems *Symp. Gyro Technology (Stuttgart, Germany)*
[6] Wang S, Yang G and Wang L 2019 An improve hybrid calibration scheme for strapdown inertial navigation system *IEEE Access* **7** 151669–81
[7] Pan J Y, Zhang C X and Cai Q Z 2014 An accurate calibration method for accelerometer nonlinear scale factor on a low-cost three-axis turntable *Meas. Sci. Technol.* **25** 025102
[8] Yuan B L, Liao D and Han S L 2012 Error compensation of an optical gyro INS by multi-axis rotation *Meas. Sci. Technol.* **23** 025102
[9] Gao J M, Zhang K B, Chen F B and Yang H B 2015 Temperature characteristics and error compensation for quartz flexible accelerometer *Int. J. Autom. Comput.* **12** 540–50
[10] Pan Y, Li L, Ren C and Luo H 2010 Study on the compensation for a quartz accelerometer based on a wavelet neural network *Meas. Sci. Technol.* **21** 105202

[11] Ban J, Wang L, Liu Z and Zhang L 2020 Self-calibration method for temperature errors in multi-axis rotational inertial navigation system *Opt. Express* **28** 8909–23
[12] Weng J 2020 Multi-position continuous rotate-stop fast temperature parameters estimation method of flexible pendulum accelerometer triads *Measurement* **169** 108372
[13] Yang Q, Zhang R and Li H 2018 Economical high-low temperature and heading rotation test method for the evaluation and optimization of the temperature control system for high-precision platform inertial navigation systems *Sensors* **18** 3967
[14] Yang H, Huang W, Jiao S, Sun X, Hong W and Qiao L 2019 Temperature independent polarization-maintaining photonic crystal fiber with regular pentagon air hole distribution *Optik* **185** 390–6
[15] Chen X and Shen C 2013 Study on temperature error processing technique for fiber optic gyroscope *Optik-Int. J. Light Electron Opt.* **124** 784–92
[16] Guo J and Zhong M 2021 Calibration and compensation of the scale factor errors in DTG POS *IEEE Trans. Instrum. Meas.* **62** 2784
[17] Chen X and Shen C 2013 Analysis and modeling for fiber-optic gyroscope scale factor based on environment temperature *Appl. Opt.* **51** 2541–7
[18] Wang Z H, Cheng X H and Fan S M 2019 Eight-position systematic calibration method for SINS based on two-axis turntable with temperature compensation *J. Chin. Inertial Technol.* **27** 23–31
[19] Liao L and Li Q 2015 Parameter identification and temperature compensation of quartz flexible accelerometer based on total least squares *Int. J. Signal Process. Syst.* **4** 27–31
[20] Xu Q L, Han B and Deng Z L 2004 Calibration method for laser strapdown inertial measurement unit in all environment temperature *J. Chin. Inertial Technol.* **12** 4–12
[21] Jiao F and Chu Z 2012 An improved six-position hybrid calibration for RLG POS in full temperature *8th IEEE Int. Symp. on Instrumentation and Control Technology (ISICT) Proc.* pp 246–50